

Chapter 2

Metallurgy of Steels



Baris Çetin and Halim Meço

Abstract In hot stamping, typically, C-Mn-B alloyed steels are used and the process involves phase transformations. Thus, a clear understanding of the effects of alloying elements, different phases of steels, and their kinematics are critical for comprehensive understanding of the process.

2.1 Phases of Steels and Their Properties

Hot stamping involves a number of phase changes during the process. The as-received material contains a “Ferritic-Pearlitic” microstructure, and then during processing, it is heated over its “Austenitization” temperature (above A_3). For the required ultra high strength, it is then quenched to form “Martensite”. As discussed in the next sections, there is also a recent trend to tailor the properties of the part by slowly quenching “soft zones” to have “Bainitic” structure which may have better elongation properties.

Based on this discussion, the properties of the five microstructures/phases involved in hot stamping process are explained in the following sections (Fig. 2.1).

Austenite

Austenite, also known as γ -iron, is the face-centered cubic (*fcc*) phase of steel, see Fig. 2.3a. This phase is typically not stable at low temperatures, although special alloying elements may stabilize austenite as in TWIP (Twinning-Induced Plasticity) steels and austenitic stainless steels. Most heat treatment operations start with austenite phase [2, 3].

B. Çetin (✉) · H. Meço
FNSS Defense Systems Co. Inc., R&D Center, Gölbaşı, Ankara, Turkey
e-mail: cetin.baris@fnss.com.tr

H. Meço
e-mail: halim.meco@fnss.com.tr

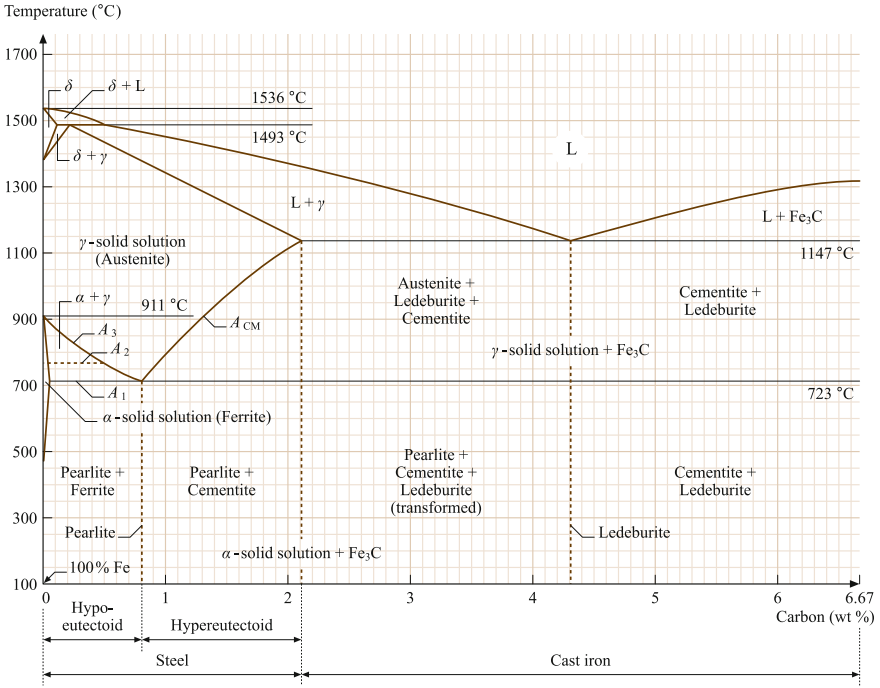


Fig. 2.1 Fe-C phase diagram [1]

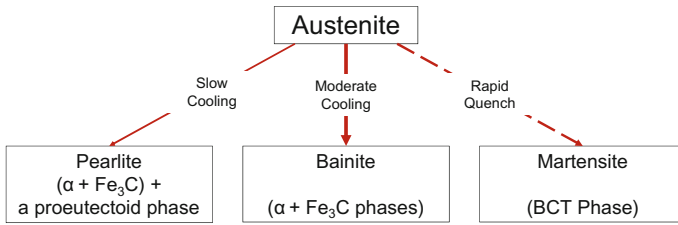


Fig. 2.2 Possible transformations of austenite: solid lines show transformation with diffusion, dashed line shows diffusionless transformation (re-created after [2])

Bainite

As shown in Fig. 2.2, if austenite is cooled at a moderate rate, bainite is produced. Bainite is not a phase, but a microstructure composed of cementite (Fe_3C) and ferrite [1, 2], which is explained in the next section.

Ferrite

Ferrite, also known as α -iron, is the body-centered cubic phase of steel, Fig. 2.3b. Low-carbon steels are mostly ferrite, whereas medium-carbon and high-carbon steels are mostly ferrite with some pearlite [2, 4].

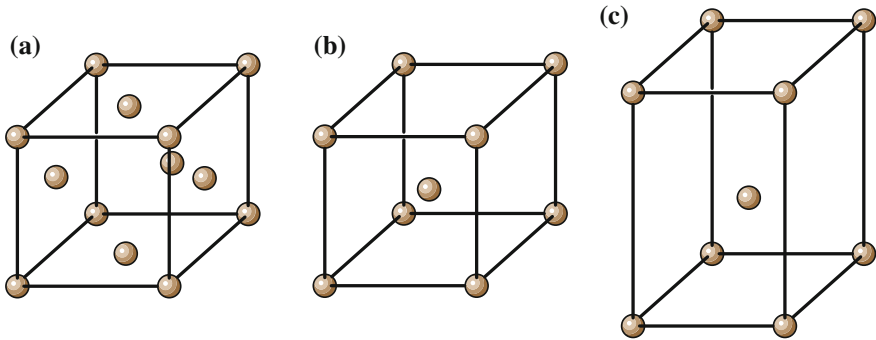


Fig. 2.3 **a** Austenite is face-centered cubic, **b** Ferrite is body-centered cubic (bcc) and **c** Martensite is body-centered tetragonal [1]

Martensite

Martensite is the hardest form of steel. This microstructure is formed by rapid cooling of Austenite, so rapid that carbon diffusion cannot take place. Because of carbon supersaturation, martensite has a larger and slightly expanded crystal structure compared to *bcc* (body-centered cubic) ferrite. The resultant martensite crystal structure is *bct* (body-centered tetragonal) as shown in Fig. 2.3c. The martensitic transformation is a diffusionless solid-state shear deformation. In steels, martensite is formed from austenite containing relatively higher amounts of carbon atoms and in view of the diffusionless nature of its formation, martensite ideally inherits the carbon atoms of the parent austenite. The carbon atoms are trapped in octahedral interstitial sites between iron atoms. In addition to the fact that the chemical composition of the austenite is directly inherited by the martensite, the martensitic shear deformation is accomplished by a plane strain shape change parallel to a set of crystallographic planes of the parent austenite. Therefore, when the martensite is formed, the volume of metal is increased, and the transformation plasticity is also produced, which directly affects the distortion and residual stress state of the final part [5, 6].

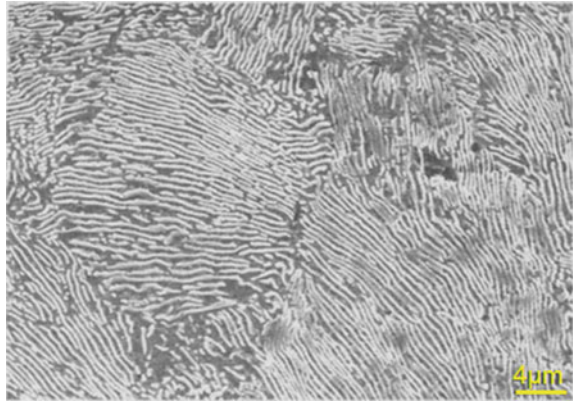
Pearlite

Pearlite microstructure is a lamellar mixture of ferrite and cementite (Fe_3C). These exist as grains, called as “pearlite colonies”. In each colony, the layers of Cementite points in the same direction, as shown in Fig. 2.4 [2].

2.2 The Effect of Alloying Elements

In plain carbon steels, the nose of the TTT (Time-Temperature- Transformation) and CCT (Continuous Cooling Transformation) curves are located at very short times; hence, very fast cooling rates are required to produce an all-martensite microstructure.

Fig. 2.4 SEM image of pearlite: white areas show ferrite and black areas show cementite [7]



In the thin sections of steel, the rapid quench produces distortion and cracking. In thick sections, it is not possible to produce fully martensitic microstructures. All common alloying elements in steel shift the TTT and CCT diagrams to longer times, permitting us to obtain all-martensite even in thick sections at slow cooling rates [8]. As alloying elements influence CCT and TTT curves, they may also alter the Martensite-start (M_s) and Martensite-finish temperatures (M_f). All alloying elements apart from Cobalt and Aluminum lower the M_s and M_f temperature [9]. For high-carbon steels, the M_f temperature generally lies below the room temperature, which means that there always exists some amount of retained austenite in the final product.

In hot stamping, typically manganese-boron alloyed steels are used. Typical hot stamping steel (22MnB5) has about 0.22% C, 1.18% Mn and 0.002% B [10]. The alloying is designed in such a way that:

- (1) the parts have high yield and ultimate tensile strength after quenching [11],
- (2) martensitic transformation can be completed in a water cooled die [11],
- (3) phase transformations are avoided during blank transfer from the furnace to the press [12],
- (4) the final parts are weldable in automotive body shops (which requires low C and Mn) [13].

In the next subsections, the effects of common alloying elements are explained individually.

Carbon (C)

As carbon content increases, steel's strength and hardness increases as displayed in Fig. 2.5, but weldability and ductility decrease. In hot stamping applications, Carbon content in the most common steel 22MnB5 is 0.22%. Steels with higher strength (i.e., 1800–2000 MPa) have even higher carbon contents up to 0.37%. Recently, energy absorbing grades for hot stamping are also introduced with carbon content between 0.10–0.12% and strength levels between 450–1000 MPa. Carbon also has an effect in phase transformations such as lowering the Martensite-start temperature, as shown in Fig. 2.6 [4, 10, 14–17].

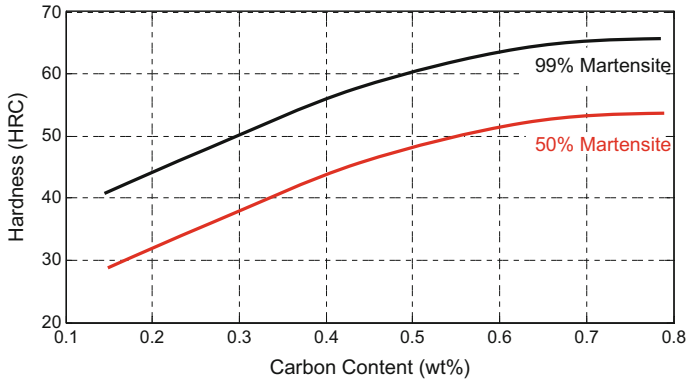


Fig. 2.5 Dependence of carbon content on hardness and martensite phase fraction (re-created after [17])

Manganese (Mn)

Manganese is found in almost all steels, at least by $\sim 0.3\%$. It is used as a deoxidizer and also reduces susceptibility to hot shortness during hot working. It also increases the hardness and hence results in a reduction in ductility as well as weldability. There is also a concurrent increase in hardenability with Mn addition. Large quantities of Mn ($>2\%$) cause cracking and distortion problems after quenching. However, after 5%, a complex microstructure with austenite at room temperature may be present. The so-called Medium-Mn (typically 5–12% Mn) and High-Mn (TWIP steels, $>15\%$ Mn) steels have both high strength and elongation for cold stamping applications. Medium-Mn steels have also been studied for hot stamping as explained in Sect. 4.4. Mn lowers the austenitization temperature, which could reduce the furnace temperature in hot stamping and thus save energy and reduce the carbon emissions during heating [4, 9, 18, 19]. In low-carbon steels, Mn retards bainite formation, which is useful for hot stamping where the final microstructure is expected to have $\sim 100\%$ martensite. Mn also reduces martensite-start temperature, but is not as effective as carbon (Fig. 2.6) [16, 20].

The steels used in hot stamping contain 0.8 to 1.3% Mn, the typical amount is around 1.2% [10, 14].

Boron (B)

Certain elements such as Ti, Al, V, Zr, and B improve the hardening properties of steel by forming carbides. Boron is the most effective of these elements. Hardenability of steels with carbon level up to 0.5% increases with even a very small amount of boron (0.001–0.003%) [1, 4, 17]. According to Zhu et al., this can be explained by segregation of free B atoms and/or borocarbide ($Fe_{23}(CB)_6$) at the austenite grain boundaries and delaying the ferrite and pearlite formation [21]. This can be seen in Fig. 2.6. Naderi et al. studied a total of nine different C-Mn alloys, five with B addition, and found out that without B-alloying, it was not possible to get 100% martensitic structure with water-cooled dies [22].

Chromium (Cr)

Chromium is used as an alloying element mainly to increase the hardenability and corrosion resistance, and also to improve the high-temperature properties such as strength and oxidation resistance. It also provides abrasion resistance in high-carbon compositions as it is a strong carbide former. Chromium is one of the major hardening elements and superior mechanical properties can be attained when used together with a toughness increasing element such as nickel. It is generally used with molybdenum when high-temperature strength is required. Hot stamping steels typically contain up to 0.30 % Cr [23–26].

Niobium (Nb)

Niobium is known to inhibit grain growth during austenitizing [9]. It is well known that for low-carbon steels “Prior Austenite Grain Size” (PAGS) improves the strength and toughness [27]. For higher strength hot stamping steels, Nb is recommended for improved toughness [28]. Another advantage of Nb is reducing the hydrogen diffusivity. This is important to reduce Hydrogen-Induced Delayed Fracture [29, 30]. The effects of Nb are also investigated in Sects. 4.2 and 6.5.

Silicon (Si)

Silicon is used as a deoxidizer in steelmaking process. Its amount depends on the steelmaking process employed and can reach to the levels of 0.15–0.30 % in fully killed steels. Silicon has a slight hardening effect on the ferrite phase and is usually detrimental to surface quality for low-carbon steels. Typically, hot stamping steels contain 0.20–0.35 % Si [23–25].

Phosphorus (P)

Phosphorus results in increased strength and hardness, however, this comes at a cost of decreased ductility and toughness. It also causes temper embrittlement in medium-carbon steels. It can be used as a deliberate alloying addition in order to increase the machinability and corrosion resistance. However, its amount should be restricted typically to 0.030 % in hot stamping steels [23–26].

Sulfur (S)

Transverse ductility and notch impact toughness characteristics suffer with increased sulfur content. Moreover, weldability also decreases with increased sulfur content. It is very detrimental to surface quality, particularly in steels containing low-carbon and low-manganese. Except for free machining steels, sulfur is considered as a detrimental element and therefore its amount is restricted typically to 0.015 % in hot stamping steels. Sulfur also has a great segregation tendency in steels and usually occurs in the form of sulfides, the most common form of which is MnS (manganese sulfide) [23–26].

Aluminum (Al)

Aluminum’s main function in steelmaking process is to deoxidize and control the grain size. It is added to steel mainly to inhibit the growth of austenite grains during heating prior to quenching. Besides aluminium, other elements such as titanium, vanadium, and zirconium are used for controlling austenite grain size, however, aluminum is the most effective element used for this purpose. Conversely, it also has adverse effects on the hardenability for heat-treatable grades as aluminum form stable carbides which are difficult to dissolve during heat treatment. Hot stamping steels contain a restricted amount of aluminum which is typically limited to 0.08% [23–26].

Nitrogen (N)

Nitrogen additions to steel results in increased strength, hardness and machinability. However, these come at the expense of decreased ductility and toughness. By forming aluminum nitrides, it acts as a grain size controlling agent in aluminum-killed steels, hence increasing both ductility and toughness. Nitrogen can reduce the effect of boron on the hardenability of steels and therefore its amount is restricted typically to 0.01 % for hot stamping steels [23–26].

2.3 Phase Transformations

To achieve ultra high strength steel at the end of hot stamping process, the transformation of austenite to martensite is required. Phase transformations take place either

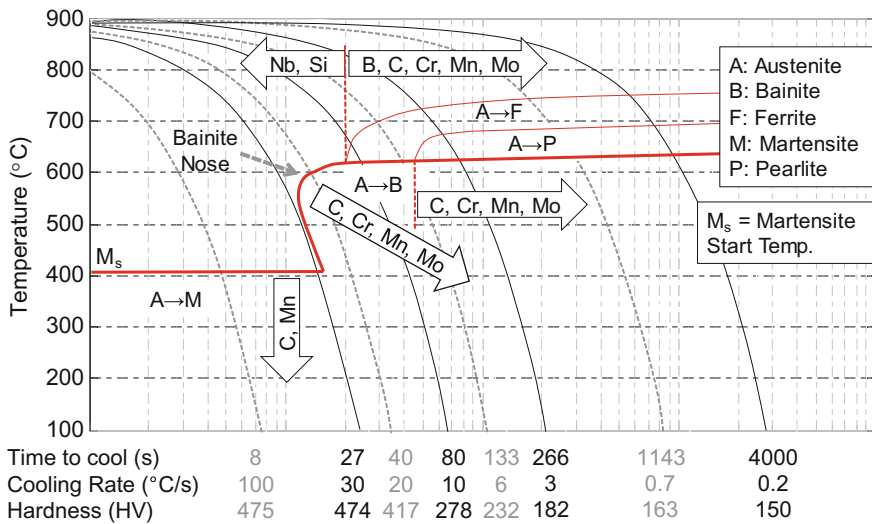


Fig. 2.6 CCT diagram for 22MnB5 steel and the effects of alloying elements (re-created from [16, 31])

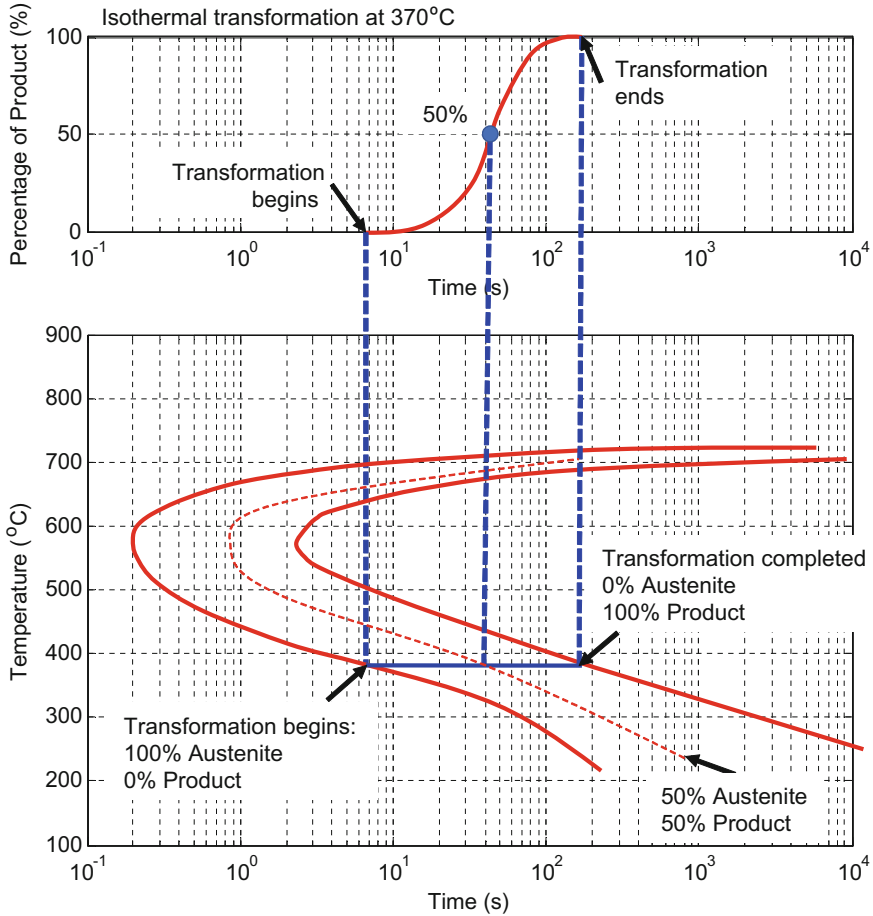


Fig. 2.7 Approximation of phase transformation by using Avrami equation (re-created after [2, 32])

during heating the steel (i.e., ferrite and pearlite transforms to austenite) or during cooling (from austenite to others).

During cooling, austenite transforms to ferrite and pearlite if cooled slowly, bainite forms at a moderate cooling rate and at high cooling rate martensite forms. As shown in Fig. 2.6, the final microstructure can be predicted by using CCT curves [2, 4, 25].

In finite element models, Avrami (also known as Johnson–Mehl–Avrami–Kolmogorov) equation Eq. (2.1) is used to model phase transformations. Coefficients of Avrami equation are b and n , for each phase, and these can be calculated by using TTT diagrams, as shown in Fig. 2.7.

$$P, B, F = 1 - \exp\left(-b * \left(\frac{t}{t_0}\right)^n\right) \quad (2.1)$$

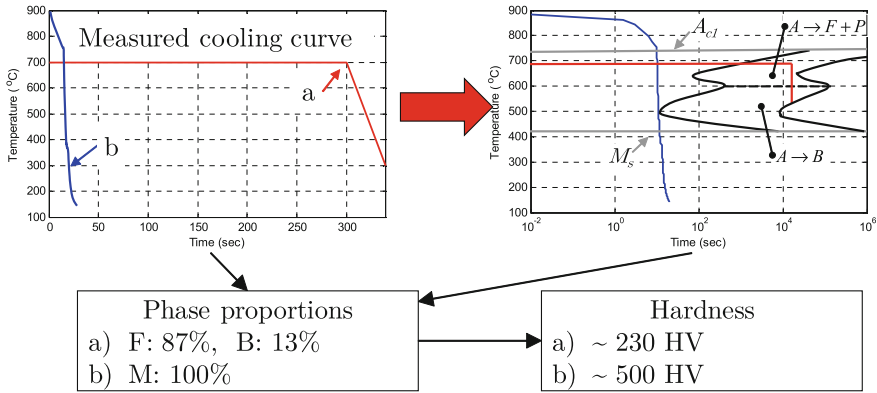


Fig. 2.8 Prediction of microstructure evolution in finite element analysis (re-created after [4, 34–36])

where, P, B, and F stand for pearlite, bainite and ferrite percentages, respectively. For each phase and at given temperature levels, b and n can be calculated using TTT curves. For martensite transformation, the equation slightly changes into Eq. (2.2):

$$M = 1 - \exp[-c * (M_s - T)^m] \tag{2.2}$$

In the literature, there are some equations which are specifically dedicated to determine the martensitic transformation such as Koistinen-Marburger equation. By this formulation, the volume fraction of transformed martensite as a function of temperature could also be computed [33].

The main factor that determines the rate in a phase transformation, such as austenite-to-pearlite transformation, is temperature. The sigmoidal-shaped curve shown in the upper portion of Fig. 2.7 gives the percentage transformation versus the logarithm of time at a specific temperature (i.e. 370 °C (700 °F)) for an iron-carbon alloy of eutectoid composition. Depending on the temperature relative to the tip of the TTT curve (approx. 580 C), varying the temperature shifts the sigmoidal curve, for example increasing temperature shifts it to the right if above the tip of TTT curve or to the left if below the tip of TTT curve. For each such curve, data is collected after rapidly quenching a specimen composed of 100% austenite to a specific temperature of interest; after which temperature is maintained constant throughout the course of the reaction.

The bottom portion of Fig. 2.7 represents another suitable way of depicting time and temperature dependence of this transformation. In this graph, two solid curves represent the time required for the start of the transformation and the finish of the transformation, respectively at a specific temperature of interest. The dashed curve that is located in the middle of start and finish curves correspond to 50% of transformation completion. These curves are typically generated from a series of plots of the percentage transformation versus the logarithm of time taken over a range of temperatures, an example of such curves is the sigmoidal-shaped curve given in

Fig. 2.7. Upper portion of Fig. 2.7 illustrates how the data transfer is made at a specific isothermal hold temperature, in this case 370 °C (700 °F) [2, 32].

FE model can use the coefficients of Avrami equation to estimate the final microstructure distribution. For example, for two different cooling conditions a and b , as shown in Fig. 2.8, it is possible to calculate the expected phase fractions upon cooling to room temperature using TTT or CCT curves. These phase fractions can then be taken into account for calculating the expected mechanical properties, in this case, hardness for cooling conditions a and b .

References

1. K.H. Grote, E.K. Antonsson, *Springer Handbook of Mechanical Engineering* (Springer, Würzburg, 2009)
2. W.D. Callister, D.G. Rethwisch, *Fundamentals of Materials Science and Engineering*, vol. 21 (Wiley, New York, 2013)
3. B.C. De Cooman, O. Kwon, K.G. Chin, State-of-the-knowledge on TWIP steel. *Mater. Sci. Technol.* **28**(5), 513–527 (2012)
4. G.E. Totten, *Steel Heat Treatment: Metallurgy and Technologies* (CRC Press, Boca Raton, 2006)
5. G. Krauss, Deformation and fracture in martensitic carbon steels tempered at low temperatures. *Metall. Mater. Trans. B* **32**(2), 205–221 (2001)
6. D. Deng, FEM prediction of welding residual stress and distortion in carbon steel considering phase transformation effects. *Mater. Des.* **30**(2), 359–366 (2009)
7. D.C. Madeleine, *The Pearlite Transformation* (Springer, Berlin, 2004), pp. 195–208
8. D.R. Askeland, W.J. Wright, *Essentials of Materials Science & Engineering* (Cengage Learning, Boston, 2013)
9. M. Maalekian, The effects of alloying elements on steels (i). *Christ. Doppler Lab. Early Stages Precip.* **23**, 221–230 (2007)
10. H. Karbasian, A.E. Tekkaya, A review on hot stamping. *J. Mater. Process. Technol.* **210**(15), 2103–2118 (2010)
11. M. Naderi, *Hot Stamping of Ultra High Strength Steels*
12. S. Bruschi, G. Liu, *Hot Stamping-Comprehensive Materials Processing* (Elsevier, Amsterdam, 2014)
13. American Society of Metals, *ASM Handbook of "Welding and Brazing"*, vol. 06, , 2nd edn. (ASM International, 1993)
14. S. Graff, T. Gerber, F.J. Lenze, S. Sikora, About the simulation of microstructure evolution in hot sheet stamping process and the correlation of resulting mechanical properties and crash-performance, in *3rd International Conference on Hot Sheet Metal Forming of High Performance Steel, CHS2, Kassel, Germany* (2011), pp. 323–330
15. ArcelorMittal Flat Carbon Europe S.A. ArcelorMittal Automotive Product Offer Europe, Android App, V1.0 (2015)
16. H. Mohrbacher, Martensitic automotive steel sheet - fundamentals and metallurgical optimization strategies, in *Innovative Research in Hot Stamping Technology*, vol. 1063. Advanced Materials Research (Trans Tech Publications, 2015), pp. 130–142
17. American Society of Metals, *ASM Handbook of "Heat Treating, 3rd printing"*, vol. 4 (ASM International, 1995)
18. H. Aydin, E. Essadiqi, I.H. Jung, S. Yue, Development of 3rd generation AHSS with medium Mn content alloying compositions. *Mater. Sci. Eng.: A* **564**, 501–508 (2013)

19. Q. Han, W. Bi, X. Jin, W. Xu, L. Wang, X. Xiong, J. Wang, P. Belanger, Low temperature hot forming of medium-Mn steel, in *5th International Conference on Hot Sheet Metal Forming of High Performance Steel, CHS2, Toronto, ON, Canada* (2015), pp. 381–389
20. W. Alqhadafi, Laser welding of boron and bainitic steels (2012)
21. Kangying Zhu, Carla Oberbillig, Céline Musik, Didier Loison, Thierry Jung, Effect of b and b+nb on the bainitic transformation in low carbon steels. *Mater. Sci. Eng.: A* **528**(12), 4222–4231 (2011)
22. M. Naderi, M. Ketabchi, Abbasi M., Bleck W., Analysis of microstructure and mechanical properties of different boron and non-boron alloyed steels after being hot stamped. *Procedia Eng.* **10**, 460–465 (2011)
23. ArcelorMittal. Extract from the product catalogue (2015). Accessed 10 June 2015
24. SSAB, Docol 22MnB5 - cold rolled boron steel for hardening in water or oil. Product Catalogue (2011)
25. J.R. Davis, *Carbon and Alloy Steels* (ASM International, 1996)
26. Salzgitter Flachstahl, 22MnB5 boron alloyed quenched and tempered steel. Product catalogue (2014)
27. C. Wang, M. Wang, J. Shi, W. Hui and H. Dong, Effect of microstructure refinement on the strength and toughness of low alloy martensitic steel. *J. Mater. Sci. Technol.* **23**(05), 659 (2007)
28. J. Wang, C. Enloe, J. Singh, C. Horvath, Effect of prior austenite grain size on impact toughness of press hardened steel. *SAE Int. J. Manuf.* **9**, 488–493, 04 (2016)
29. H. Mohrbacher, Influence of alloy modifications and microstructure on properties and crash performance of press hardened steel components, in *6th International Conference on Hot Sheet Metal Forming of High Performance Steel, CHS2, Atlanta, GA, USA* (2017), pp. 213–222
30. S. Tateyama, R. Ishio, K. Hayashi, T. Sue, Y. Takemoto, T. Senuma, Microstructures and mechanical properties of V and/or Nb bearing ultrahigh strength hot stamped steel components. *Tetsu-to-Hagane* **100**(9), 1114–1122 (2014)
31. L. Vaissiere, J.P. Laurent, A. Reinhardt, Development of pre-coated boron steel for applications on PSA Peugeot Citroën and Renault bodies in white, in *SAE Technical Paper*, vol. 7. (SAE International, 2002)
32. American Society for Metals. Ohio. *Atlas of Isothermal Transformation and Cooling Transformation Diagrams* (Metals Park, Ohio, 1977)
33. C. Şimşir, C.H. Gür, An FEM based framework for simulation of thermal treatments: application to steel quenching. *Comput. Mater. Sci.* **44**(2), 588–600 (2008)
34. F.F. Li, M.W. Fu, J.P. Lin, Effect of cooling path on the phase transformation of boron steel 22MnB5 in hot stamping process. *Int. J. Adv. Manuf. Technol.* **81**(5), 1391–1402 (2015)
35. G.-Z. Quan, T. Wang, L. Zhang, Research on the influence of hot stamping process parameters on phase field evolution by thermal-mechanical phase coupling finite element. *Int. J. Adv. Manuf. Technol.* **89**(1), 145–161 (2017)
36. C. Koroschetz, K. Eriksson, O. Kragt, A. Ademaj, Production method for locally, graded presshardened components through process integration of a heating technology in combination with appropriate process control, in *IDDRG 2016, Linz, Austria* (2016), pp. 356–362